[Short title + Author Name - P&H title] 17 (2024) 106036

Contents lists available at ScienceDirect

Arabian Journal of Chemistry

journal homepage: www.ksu.edu.sa

Original article

Preparation of modified silica gel supported silver nanoparticles and its evaluation using zone of inhibition for water disinfection

Belete Tessema [a], Girma Gonfa [a,b,c,*], Sintayehu Mekuria Hailegiorgis [a]

[a] Department of Chemical Engineering, Addis Ababa Science and Technology University, 16417 Addis Ababa, Ethiopia
[b] Biotechnology and Bioprocess Center of Excellence, Addis Ababa Science and Technology University, 16417 Addis Ababa, Ethiopia
[c] Nanotechnology Center of Excellence, Addis Ababa Science and Technology University, 16417

ARTICLE INFO

Keywords:
Teff straw
Teff straw ash
Silica gel
Modified silica gel
Silver nanoparticles

ABSTRACT

In this work, preparation of modified silica gel supported silver nanoparticles and its evaluation using zone of inhibition for water disinfection were investigated. The silica contents of the teff straw [TS] and teff straw ash [TSA] are 5.92 and 92.21 %, respectively. The calcinated TS ash at 700 °C was mixed with NaOH solution. The solution is then neutralized with HCl solution and then gel formation using the sol gel method. The silica gel yield was recorded and characterized. The SG with major silica functional group, amorphous structure, high porosity from the morphology, high surface area of 807.163 m^2/g, pore volume of 0.34 cm^3/g, pore diameter of 1.70 nm and silica gel purity of 99.39 % were achieved at a calcination temperature of 700 °C. It is then; further modified using trimethylchlorosilane (TMCS)/ethanol/hexane at different volumetric ratio and the resulting product is modified silica gel (MSG). MSG has excellent hydrophobic properties that have been required during water treatment. In this method, MSG with a major silica functional group, well ordered structure due to the TMCS modifier, maximum surface area of 510.40 m^2/g was achieved at volumetric ratio of 0.25:0.25:1 of TMCS/ethanol/hexane, respectively. Then, MSG supported AgNPs (MSG-AgNPs) was prepared by mixing different concentrations of AgNPs-MSG and characterized. The MSG-AgNPs have shown AgNPs on the surface of MSG from the EDX result, different absorbance, pore from the morphology, with a maximum surface area of 475.0 m^2/g was obtained at 1.5 mM of AgNPs concentrations. The performance of MSG-AgNPs was evaluated using zone of inhibition measurement and batch disinfection studies against *E. coli* and *S. aureus*. At 1.5 x 10^8 CFU/mL initial bacterial concentrations, the maximum inhibition zone diameter was 12.80 and 14.30 mm for *E. coli* and *S. aureus*, respectively.

1. Introduction

Waterborne pathogens are significant concern for public health, they are capable of causing diseases upon contaminating groundwater and surface water sources. These pathogens may be interred into water systems through various channels, such as human or animal waste, agricultural runoff, sewage leaks, and natural disasters. Among the most prevalent waterborne bacteria are *Escherichia coli, S. aureus, Shigella* spp., *Salmonella* spp., *Vibrio* spp., and *Cryptosporidium*. The consumption of water infected by these bacteria can affect the gastrointestinal tract, skin, bloodstream, and other bodily organs (Shayo et al., 2023; Alegbeleye and Sant'Ana, 2020; Tessema et al., 2024). *E. coli* is commonly found in the digestive tracts of mammals and a crucial indicator of fecal pollution. Its exclusive presence in mammals, including humans, signifies the recent contamination of water sources.

The treatment of drinking water often involves the use of various chemicals to mitigate bacterial contamination. Commonly employed substances include free chlorine, iodine, chloramines, and ozone. While these agents are effective in disinfection, they are not without drawbacks. A significant concern is their tendency to react with natural organic matter or other substances present in water, leading to the formation of disinfection byproducts (DBPs). Some DBPs have been identified or are suspected to be carcinogenic, posing an increased risk of cancer to humans (El-Aassar et al., 2013; Phong et al., 2009; Tessema et al., 2024; Hussain, et al., 2022).

Metal nanoparticles are used in water treatment, attributed to their distinctive physical and chemical characteristics. Among the most prevalent metal nanoparticles such as silver, zinc, copper, gold, cerium

* Corresponding author at: Department of Chemical Engineering, Addis Ababa Science and Technology University, 16417 Addis Ababa, Ethiopia.
E-mail address: kiyyaagonfaa@gmail.com (G. Gonfa).

https://doi.org/10.1016/j.arabjc.2024.106036
Received 25 April 2024; Accepted 23 October 2024
Available online 28 October 2024
1878-5352/© 2024 The Author(s). Published by Elsevier B.V. on behalf of King Saud University. This is an open access article under the CC BY-NC-ND license (http://creativecommons.org/licenses/by-nc-nd/4.0/).

dioxide, and titanium dioxide (Ojha, 2020; Neme et al., 2023; González-Castaño et al., 2021; Khan, 2023; Anjum et al., 2022; Khan et al., 2022; Khan et al., 2021; Rahmanifar et al., 2024). One of the most significant and intriguing nanomaterials that are employed in water disinfection is AgNPs. The use of AgNPs in water treatment processes not only ensures the removal of harmful pathogens but also contributes to the safety and sustainability of water resources. Their unique characteristics, such as a high surface area-to-volume ratio and the ability to release silver ions, enable them to target and neutralize microbes efficiently (Khan, 2023; Zhang et al., 2016; Payami et al., 2016).

Despite the promising applications of AgNPs in water purification, several obstacles hinder their widespread adoption. The propensity of AgNPs to aggregate reduces their effectiveness, while concerns about their stability, toxicity, and environmental footprint raise significant issues. Notably, the release of silver ions during water treatment poses risks to both ecological systems and human health. Consequently, it is imperative to advance research focused on enhancing the stability and reducing the hazardous effects of AgNPs to ensure they are a viable option for water treatment technologies (Payami et al., 2016; Thamilselvi and Radha, 2017; Bruna et al., 2021). To increase the efficacy of water disinfection using AgNPs, it is advantageous to incorporate them with a variety of materials. These include polymers, granular activated carbon, known for its adsorption capabilities; ceramic filters; filter membranes; and silica, which can act as a stabilizing agent. This integration not only restricts the aggregation of AgNPs but also enhances their stability and reusability, leading to an extended lifespan and reduced operational costs in water treatment systems (Quang et al., 2013; Tabrez and Khan, 2022; Khan et al., 2022; Tesfaye Gari et al., 2023). Silica-based materials are particularly suitable for stabilizing nanoparticles for biological applications, as they have several advantages such as biocompatibility, high chemical and thermal stability, and hydrophilic nature. Also, the SiO_2 surface has many hydroxyl groups that contribute to its stability in water-based solutions. So far, researchers have used nanoparticles to coat them with a mesoporous SiO_2 layer (Sarker et al., 2021; Parandhaman et al., 2015).

The industrial synthesis of silica necessitates elevated thermal conditions, often reaching up to 1700 °C, which underscores the challenges of commercial scalability. Prolonged inhalation of crystalline silica dust can precipitate silicosis, a condition that has been linked to severe respiratory ailments such as lung cancer, emphysema, and pulmonary tuberculosis (Raanan et al., 2022; Murugadoss et al., 2017). As a result, considerable interest has been drawn to the quest for alternate reduction origins and predecessors. Due to this limitation, silica gel-rich precursors, such as rice husk, bamboo leaf, rice straw, sugarcane bagasse, wheat straw, maize leaves, and teff straw (Tessema et al., 2023 (2023).; Gari et al., 2024; Asfaw et al., 2024) were used.

The synthesis of silica gel from biomass resources presents a multitude of benefits, notably the reduction of production costs and the enhancement of environmental sustainability (Morales-Paredes et al., 2023; Bageru and Srivastava, 2018; Azarang et al., 2021). In Ethiopia teff straw was produced over two million tons annually (Tessema et al., 2023; Tessema et al., 2023). Moreover, TS is regarded as a promising and affordable bio-precursor for the production of silica gel. In previous study, silica gel was prepared from a variety of *sergegna* (white and brown mixed) TS with unknown species via the sol–gel method, obtaining a yield of 91 to 92 % (Bageru and Srivastava, 2018; Tessema et al., 2023).

This research work addresses the synthesis of silver nanoparticles (AgNPs) from *Vernonia amygdalina* leaf extracts with the integration of modified silica gel (MSG). Utilizing plant extracts are used for reducing and stabilizing agents for synthesis of AgNPs. Also synthesizing green AgNPs is environmentally friendly and cost-effective. The incorporation of MSG, achieved through the sol–gel method, strengthens the stability and dispersibility of AgNPs. Concurrently MSG-AgNPs is amplifying antimicrobial efficacy against a spectrum of pathogens such as *E. coli* and *S. aureus*. Previously, the antibacterial potency of AgNPs-enriched MSG in zone of inhibition assays against bacteria remains unexplored. This study endeavors to bridge this knowledge void.

2. Materials and methods

2.1. Chemicals and materials

Filagot (red) teff straws were obtained from the Debre Zeit Research Centre, Ethiopia. The teff straw was transported to the Ababa Science and Technology University laboratory in a polyethylene bag. Loba Chemie Pvt. Ltd. provided the hydrochloric acid (HCl, 37 %). (India). The sources of 96 % of sodium hydroxide (NaOH) from Abron Chemicals Ltd. in India. We purchased 99.9 % anhydrous ethanol (EtOH) from Favor Trading plc in Taiwan. The source of aqueous ammonia ($NH_3{\cdot}H_2O$, 30 %) was Neolab Pvt. Ltd. The source of the trimethylchlorosilane (C_3H_9ClSi, 98 %, Cisco Research Laboratory Pvt. Ltd., USA) was the same as mentioned above. The acquired N-hexane (C_6H_{14}, 99 %) from Atico (India). The chemical analyses were performed to determine the composition of the teff straw. The compositions of the TS and TSA were carried out using atomic absorption spectroscopy (CB-AAS-3510).

2.2. Methods

2.2.1. Teff straw sample preparation

TS underwent a meticulous cleaning process to ensure the removal of all impurities, including leaves, sand, dirt, and clay. This involved an initial soaking in tap water for a full 24 h, followed by a thorough washing sequence where the straw was rinsed five times with tap water to remove any remaining dirt and waste. Subsequently, the straw was left to dry naturally under the sun's warmth. Once completely dried, the straw was processed through a high-speed grinder to achieve a fine powder with a particle size of 2 μm or smaller. This finely ground powder was then carefully stored in sealed polyethylene bags to maintain its purity until needed for further applications. Grounded teff straw (50 gm) was subjected to 2.5 N acid (250 mL) leaching by treating it with hydrochloric acid at a temperature of 80 °C for a duration of one hour under continuous stirring.

2.2.2. Preparation of teff straw ash

Teff straw ash was produced using the method reported by Tessema et al (Tessema et al., 2023) and Tessema et al (Tessema et al., 2023), with some modifications. The process involved the careful selection of high-quality teff straw, which was then subjected to controlled combustion to ensure complete ashing. Calcination is a thermal treatment process applied to the acid-treated teff straw in a controlled environment within a programmable muffle furnace. This process involves heating the straw to a high temperature of 700 °C for a duration of 2 h, causing the decomposition of organic materials and inducing physical and chemical changes. The purpose is to remove volatile substances, reduce moisture content, and alter the physical properties of the straw, resulting in fine ash. Post-calcination, the ash is cooled in desiccators to prevent moisture absorption and then sealed in an airtight container to preserve its quality until needed (Tessema et al., 2023; Tessema et al., 2023).

2.2.3. Silica gel preparation

Silica gel was produced using the method reported by Tessema et al (Tessema et al., 2023) and Tessema et al (Tessema et al., 2023), with some modifications. Teff straw ash (10 g) was carefully measured and transferred into 250 mL Erlenmeyer flasks. Subsequently, 80 mL of 2.5 N NaOH solution was added to each flask. To prevent contamination, the flasks were securely covered with aluminum foil. The contents were then subjected to heating at a precise temperature of 90 ± 5 °C for a duration of 1 h, with constant magnetic stirring to ensure uniform treatment. Following the heating process, the solution was allowed to cool down to room temperature before being filtered through Whatman No. 41 ash-

less filter paper. To remove any remaining impurities, the filtered solution was washed with 100 mL of boiling water. This NaOH treatment is crucial as it facilitates the leaching of silica from the ash, resulting in the formation of sodium silicate, as illustrated in Eq. (1) (Norsuraya et al., 2016).

$$SiO_2(ash) + 2NaOH \rightarrow Na_2SiO_3 + H_2O \quad (1)$$

The filtrate was heated on a hot plate at a temperature of 90 ± 5 °C for 1 h and then cooled to room temperature. The cooled filtrates were titrated with a solution of 2.5 N HCl with a magnetic stirrer until the pH was reduced from 13.3 to 7. When pH became below 10, the silica gel started to precipitate, and the mechanism is depicted in Eq. (2) (Norsuraya et al., 2016).

$$Na_2SiO_3 + 2HCl \rightarrow SiO_2 + 2NaCl + H_2O \quad (2)$$

The solution was aged in the mother solution at room temperature for 20 h to obtain silica gel. To remove the salt (NaCl), the precipitate silica gel was repeatedly rinsed in distilled water. Then, distilled water was added and heated to 35 °C with mechanical stirring to break down the formed slurry. Next, the slurries were centrifuged for 15 min at 2500 rpm; the clear supernatant was discarded, and the washing step was repeated. Finally, the silica gel was placed in a beaker and dried at 90 °C for 12 h. The dried silica gel was ground into powder using a pestle and mortar and stored in an airtight polyethylene bag for further use.

2.2.4. Modified silica gel preparation

The method referred to involves the gradual addition of hydrochloric acid (HCl) to an aqueous sodium silicate solution, initially at a pH of 13.5. This process is detailed in Section 2.2.3, where the solution is prepared and then acidified until the pH drops to between 4 and 4.5. Rapid addition with continuous agitation is critical to prevent gelation during this stage. Following acidification, the solution is introduced to a 1 M aqueous ammonia solution, which increases the pH to 5–6, inducing gel formation. The final step to enhance the gel structure involves aging the gels for 24 h at 50 °C, as reported by Abdul Halim et al. (Abdul Halim et al., 2016). Sodium ions were removed from the gel by passing water vapour through the hydrogels using the method reported by Gurav et al. (Gurav et al., 2009). To remove the water from the pores, the prepared silica wet gels were submerged in ethanol and shaken in a water bath for 12 h at 50 50 °C (Mohamad et al., 2020; Waqas et al., 2022). In this process, ethanol acts as a solvent to extract certain compounds from the silica gel. The mixture is then treated with hexane, which helps to separate the ethanol from these compounds over an extended period of 12 h.

For surface modification, the silica wet gel was submerged and kept in a sonicator in a water bath for 12 h at 50 °C in a solution of trimethyl chlorosilane (TMCS), ethanol, and hexane. TMCS is used to modify the surface of silica gel with gain hydrophobic property. TMCS, ethanol, and hexane in various ratios (15/25/100, 25/25/100, 35/25/100, and 50/25/100 for the TMCS/ethanol/hexane ratio) were used. The TMCS-treated silica gel was first dried for 2 h at 80 °C in an oven to remove any lingering TMCS and the other solvents. It was then added to 500 mL of distilled water and sonicated for 10 min. Next, it was dried for 18 h at 85 ± 5 °C, then for 6 h at 145 ± 5 °C, and finally for 24 h at 50 ± 5 °C, as suggested by (Quang et al., 2011; Feng et al., 2018; Tessema et al., 2024). Finally, the prepared modified silica gel was grounded using a mortar for further analysis and use. The modification of the silica gel enhances its properties, making it suitable for specialized analytical techniques that require a particular surface chemistry to interact with specific substances. Therefore, the preparation and grounding of the modified silica gel are crucial steps that significantly impact its effectiveness in research and industrial applications.

2.2.5. Synthesis of silver nanoparticles

The AgNPs were synthesized utilizing the extract from Vernonia amygdalina leaves. Initially, the foliage was meticulously cleansed with distilled water and left to desiccate in shade for a septenary period. Subsequently, the arid leaves were pulverized using a coffee mill. In the ensuing step, a 250-mL Erlenmeyer flask was charged with 200 mL of distilled water and 20 g of the powdered leaf, then brought to ebullition for 20 min at a temperature of 90 ± 5 °C. Conclusively, the concoction was subjected to vacuum filtration via Whatman filter paper (No. 1, 90 mm, UK) and conserved in a refrigeration unit at 4 °C until needed for the AgNPs' synthesis.

For the synthesis of AgNPs, Vernonia amygdalina leaf extract (10 mL) was added to each containing $AgNO_3$ (1.5, 3, 6, and 9 mM) in 100 mL of distilled water. The flasks were then placed on a hot plate, and the temperature of the water was maintained at 65 ± 5 °C for 15 min with continuous magnetic stirring. The transition in the solution's color from colorless to light gray indicated the formation of AgNPs. Upon observing this color change, the flasks were promptly removed from the heating plates. To prevent the AgNPs from aggregating, the flasks were kept under a magnetic stirrer as the solutions cooled to room temperature. Subsequently, the samples were refrigerated at 4 °C for 24 h and subjected to ultrasound waves (Sonorex Digiplus DL-Ultrasonic Baths, Bandelin, Germany) for 15 min. After cooling and stirring until a light gray colloidal solution was obtained, it was confirmed that the reduction process of AgNPs was successful (Khojasteh-Taheri et al., 2023). Then, centrifuging at 5000 rpm for 10 mins for further purification of AgNPs.

2.2.6. Preparation of modified silica gel supported silver nanoparticles

Modified silica gel-supported silver nanoparticles (MSG-AgNPs) were synthesized through the impregnation method, where AgNPs were deposited onto the surface of modified silica gel. The process involved combining the modified silica gel with AgNPs in varying ratios. Specifically, 10 g of modified silica gel were treated with AgNPs synthesized at different concentrations of aqueous silver nitrate ($AgNO_3$), namely 1.5, 3, 6, and 9 mM, as detailed in Section 2.2.5 of the methodology. The mixture of silica gel and AgNPs solution was then subjected to continuous stirring on a hot plate equipped with a magnetic stirrer for a duration of 4 h at ambient temperature. Following this, the mixture was allowed to cool to room temperature before being filtered using Whatman No. 41 ash-less filter paper. To ensure the removal of any unattached AgNPs, the slurry form of MSG-AgNPs was thoroughly washed with distilled water. Finally, the filtered product was transferred to an airtight container and left to dry for 24 h at a controlled temperature of 90 ± 5 °C (Feng et al., 2018). Finally, the sample was meticulously ground using a mortar and pestle, then carefully packed into a polyethylene bag for subsequent analysis and utilization. The resultant modified silica gel supports, impregnated with AgNPs synthesized at concentrations of 1.5, 3, 6, and 9 mM, were systematically labeled as A, B, C, and D, respectively.

2.2.7. Agar well diffusion experiments

38g of brain–heart infusion broth were added to 1000 mL of distillate water that had been sterilized before being autoclaved. The e. Coli and S. Aureus cultures were then incubated at 37 °C for 24 h to get the strains to the exponential growth phase after being infused into fresh medium. Following their removal from the effluent, the cells were centrifuged for five minutes at 10,000 rpm, rinsed in sterile distillate water, and then centrifuged again before being resuspended in sterile water. A solution containing 1 % H_2SO_4 and 1 % barium chloride dihydrate was used to create a 0.5 McFarland turbidity standard. The cultures were taken out of colonies by touching them with a loop and putting them in saline, or they were taken out of broth suspension and put in saline before being adjusted to meet a 0.5 McFarland standard. This was accomplished by comparing the appearance of black lines through the inoculum under well-lit settings. In a solution that has been appropriately adjusted, the most often isolated organisms are predicted to have 1.5 x 10^8 colony forming unit (CFU)/mL. Then, 100 μm of S. Aureus and e. Coli were harvested for every 24 h that the bacteria grew on the media. Regarding

the altered silica gel-based. Then, each sample was meticulously resuspended in distilled water that had been solvent-sterilized. The samples were then subjected to sonication and autoclaving, which guaranteed the formation of a uniform solution of the modified silica gel-supported AgNPs (Wang et al., 2014; Shin et al., 2014)

The experiment was conducted in accordance with the Clinical and Laboratory Standards Institute (CLSI) M100 guideline, with a few minor modifications to take into consideration the specific experimental circumstances (Satlin et al., 2020; Khan et al., 2020). Subsequently, the modified silica gel-supported silver nanoparticles (MSG-AgNPs) samples were labeled A, B, C, and D. Then, these samples were dispersed in solvent-sterilized distilled water to achieve concentrations ranging from 2.5 to 50 mg/mL (MSG-AgNPs/water). This solution was subjected to sonication followed by autoclaving, employing the method previously described in the literature (Wang et al., 2014; Shin et al., 2014; Khan et al., 2021). The samples were put in an autoclave and the medium was autoclave sterilized for 15 min at 121 °C. After that, the medium was placed in a shaking incubator at 37 °C and 150 rpm. Next, in the sterile setting of the biological safety cabinet (BIOBASE, Chia), the sterilized medium (20 mL) was aseptically placed onto sterile, 90-mm-diameter petri dishes, cooled to a molten state, and then allowed to cool to room temperature. Following a 24-hour incubation period at 37 °C in brain–heart infusion broth, both *E. Coli* and *S. aureus* bacterial strains were suspended in sterile nutritional broth with the 0.5 MacFarland standard adjusted.

The specified test microorganisms (100 μL each) were swabbed into sterile plates containing Mueller-Hinton agar using sterile cotton swabs. After swabbing, the Mueller-Hinton agar was dried. Wells with an 8-mm diameter were punched on the inoculated agar media with the help of blue tips. Within 15 min, add 100 μL of each sample of A, B, C, and D in solution into the wells. Likewise, the distilled water of 100 μL and gentamycin of 100 μL was pipetted for negative and positive controls, respectively. All dishes were pre-incubated at room temperature for 2 h. It is used to allow uniform diffusion of the MSG-AgNPs solution into the agar medium and is then incubated at 37 °C for 24 h for both bacteria strains. The antibacterial activity was evaluated by measuring the bacterial growth inhibition zone diameter in mm. The experiments were performed in triplicate (Wang et al., 2014; Shin et al., 2014). Both growth and sterility quality controls were conducted in parallel in every experiment. Measurements were made in triplicate, and average values are reported.

2.3. Characterization

2.3.1. TS, and TSA

The proximate analyses of the TS were conducted to determine the amounts of moisture, volatile matter, ash, and fixed carbon. In this study, measurements were made in triplicate, and average values were reported. The moisture content of the sample was determined by applying the standard test method, ASTM D 3173 (International, 2017). The volatile matter contents were determined using ASTM D-3175 (Designation, 2017). And also, the ash content was determined using ASTM D-3174 (ASTM, 1988). A thermographic analyzer (SDT Q600) was used to perform the thermogravimetric analysis (TGA) of the TS. The FTIR analysis was carried out using the FTIR spectrum (Thermo Scientific ATR-FTIR, IS50) over a range of 4000–400 cm^{-1} of the TS.

To ascertain the composition of the TSA, chemical analyses were conducted. The composition of the ashes was determined using atomic absorption spectroscopy (CB-AAS-3510). Finally, TSA has been cooled inside desiccators to room temperature and kept in an airtight container until further use. The surface area of teff straw ash was determined using Brunauer-Emmett-Teller (SA-9600 series, HORIBA, USA). An X-ray diffractometer (RIGAKU-Model Ultima-IV, USA) was used to determine the determine the crystallinity of the ash.

2.3.2. Silica gel, modified silica gel and modified silica gel supported AgNPs

The study of adsorbent materials often involves a detailed analysis of their physical properties to understand their effectiveness in various applications. One common method to assess the surface area and porosity of these materials is through the Brunauer-Emmett-Teller (Amibo et al., 2022.) and Barrett-Joyner-Halenda (BJH) methods. These techniques typically utilize instruments like the Nova 4000e from Quantachrome, USA, which performs nitrogen adsorption measurements. In addition to surface characterization, MSG-supported AgNPs were analyzed using advanced UV spectroscopy techniques. For this purpose, an automated Jasco V-770 UV–vis spectrophotometer, operating at ambient conditions and provided by JASCO Co., Tokyo, Japan, was employed. The spectrophotometer was specifically tuned to scan wavelengths ranging from 200 to 600 nm, allowing for a comprehensive analysis of the nanoparticles' optical properties. An essential tool for determining the functional groups on the AgNPs supported by silica gel was the Thermo Scientific FTIR, model IS50. These groups were detected within the spectral range of 4000–400 cm^{-1}, indicative of the chemical composition of the synthesized nanoparticles. Additionally, the dried powders underwent FTIR spectroscopic analysis to further elucidate their molecular structure. The crystallinity of the samples was confirmed through X-ray diffraction analysis, employing a RIGAKU Ultima-IV system. Surface morphology studies were conducted using a JEOL JSM-6390 SEM, complemented by energy-dispersive X-ray spectroscopy (EDX) in secondary electron image mode across an accelerating voltage range of 0–15 kV. This provides detailed insights into the topography and elemental composition of the MSG-supported AgNPs. These comprehensive characterization methods have collectively contributed to a deeper understanding of the silica gel supported AgNPs.

3. Results and Discussion

3.1. Proximate analysis

The proximate analysis results are given in Table 1. Proximate analysis results showed ≈ 6 % ash and the rest 94 % as moisture, volatile matter, and fixed carbon in teff straw. Biosilica can be synthesized from the ash content after removing the rest of it.

3.2. Chemical composition result of Filagot teff straw variety

Table 2 presents the chemical composition of major and minor oxides in the Filagot variety of teff straw, among other samples. The compositional analysis was conducted using atomic absorption spectroscopy, which identified SiO_2 as the predominant oxide across all samples. Additionally, trace quantities of Fe_2O_3, CaO, K_2O, P_2O_5, and H_2O were detected, alongside minute elements of Al_2O_3, Na_2O, TiO_2, and MgO. The term LOI stands for Loss on Ignition, which is a process that occurred during the quantification of silica content.

The silica content of the raw red teff straw ash from Filagot was 92.19 %. Among the metallic oxides analysed in this study, silicon dioxide was the most abundant in all teff straw ash sample, regardless of the species. The red teff straw ash from Filagot had the highest silicon dioxide content. The second most abundant metallic oxide was MgO, followed by CaO. After neglecting the volatile matter and compared with other metallic oxides the silica content of the TSA was more than 92 %.

Table 1
Proximate analysis the average results of Filagot variety raw teff straw.

Proximate analysis (%)	
Moisture	7.39
Volatile	80.59
Ash matter	6.00
Fixed carbon in	13.39

Table 2
Chemical composition of Filagot teff straw ash.

Oxides	SiO_2	Al_2O_3	Fe_2O_3	CaO	MgO	Na_2O	K_2O	MnO	P_2O_5	TiO_2	SO_3	Other
Wt. %	92.19	0.15	0.15	3.73	2.79	0.15	0.15	0.30	0.15	0.15	–	0.09

3.3. Thermo Gravimetric and Differential thermal analysis of Filagot teff straw variety

Three separate zones of weight loss may be identified from the sample's TGA curve was presented in Fig. 1: room temperature to 112 °C, 230 °C to 400 °C, and 400 °C to 520 °C. These areas correlate to the following processes: the emission of volatile matter, the evaporation of moisture, and the combustion of combustible elements. The second section showed a notable high percentage of mass loss, which is explained by the carbon's conversion to CO and CO_2 gasses. This phenomenon is further explained by the DTG curve was presented in Fig. 1, which shows that the rate of mass loss from moisture evaporation is represented by an initial peak at 110 °C. Subsequently, at around 300 °C, the rate of volatile matter loss from teff straw reaches its maximum. After that, a positive peak appears at about 400 °C, which represents the mass loss rate as flammable organic material breaks down. Past this temperature, there is a slight mass loss rate between 500 °C and 600 °C, and then there is no discernible mass loss. It is crucial to remember that the ashing temperature for teff straw samples was determined in accordance with these TGA results in order to guarantee the extraction of high-purity biosilica by eliminating as much carbon and other impurities as feasible. Furthermore, these findings imply that the sample's combustible and carbonaceous composition degrades prior to reaching the 500 °C ashing temperature (Braschi et al., 2016).

3.4. Fourier transforms infrared spectroscopy of varieties of teff straw and ashes

The functional groups of teff straw and its ash were examined by FTIR spectroscopy. A known amount of the sample was placed on a copper grid and dried under dark conditions to remove the ethanol solvent. The FTIR spectra of the teff straw between 400 and 4000 cm^{-1} at ambient temperature revealed the presence of various functional groups in the biomass. The teff straw sample from a variety of Filagot were analyzed, and the results are shown in Fig. 2. The peak at 3380 cm^{-1} corresponds to the OH stretching vibration of the teff straw. The C = O stretching vibration is indicated by the peak at 1600 cm^{-1}, while the C–H stretching vibration is shown by the band at 2923 cm^{-1}. The strong absorption peaks at 1400 cm^{-1} are attributed to the Si-O-Si asymmetric vibration and shear modes, which are due to the high ionic character of the Si-O bond (Tessema et al., 2023).

The FTIR spectrum of the ashes obtained from the combustion of teff straw from Filagot is presented in Fig. 2. The presence of Si in the ash is indicated by the peak at 800 cm^{-1}, which corresponds to the symmetric stretching mode (Bageru and Srivastava, 2017; Bilgic et al., 2022). The Si-O bending band vibration is a fundamental vibrational mode observed in silicate minerals, which is typically represented by an absorption band at 470 cm^{-1} in infrared spectroscopy (Ding and Su, 2012). The Si-O group exhibits a more pronounced ionic character compared to other groups within the sample. This characteristic implies that the Si-O bond is significantly more polarized. Notably, the spectral peak observed at 1044 cm^{-1} can be ascribed to the Si-O-Si asymmetric stretching and bending modes. These modes are indicative of the Si-O-Si angle's deformation and the oxygen atom's displacement along the bond axis (Bageru and Srivastava, 2017). The analysis of the FTIR spectrum revealed significant differences between the teff straw and its resultant ashes. Notably, the characteristic peaks within the 3750–2500 cm^{-1} range, typically associated with hydroxyl groups in organic compounds, were conspicuously absent in the ash sample. This observation strongly suggests that the water content and organic constituents containing hydroxyl groups were effectively removed from the biomass during the thermal treatment (Amibo et al., 2022.; Bageru and Srivastava, 2017).

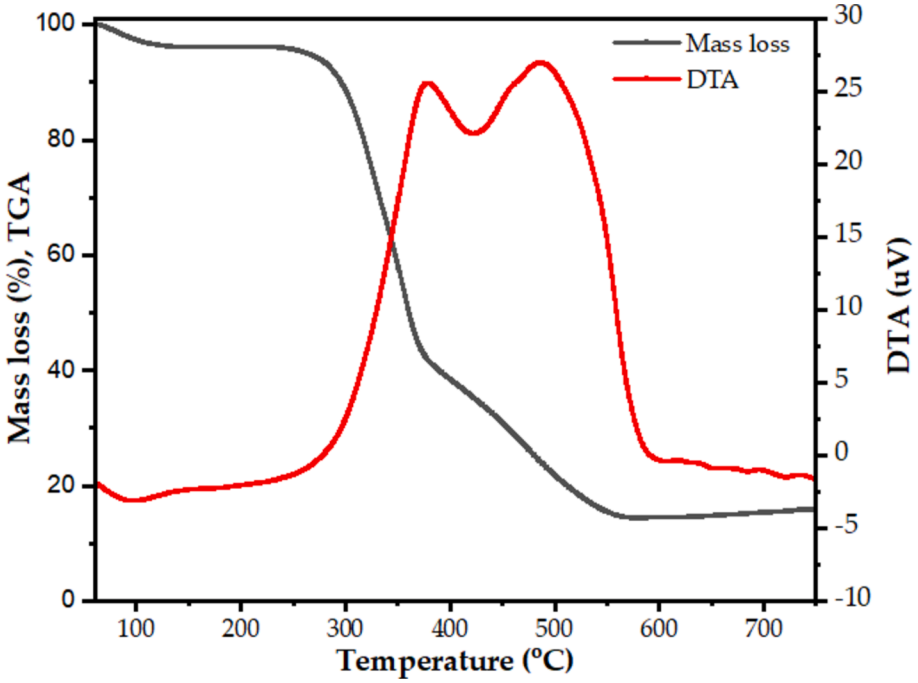

Fig. 1. TG-DTG curves of Filagot teff straw variety.

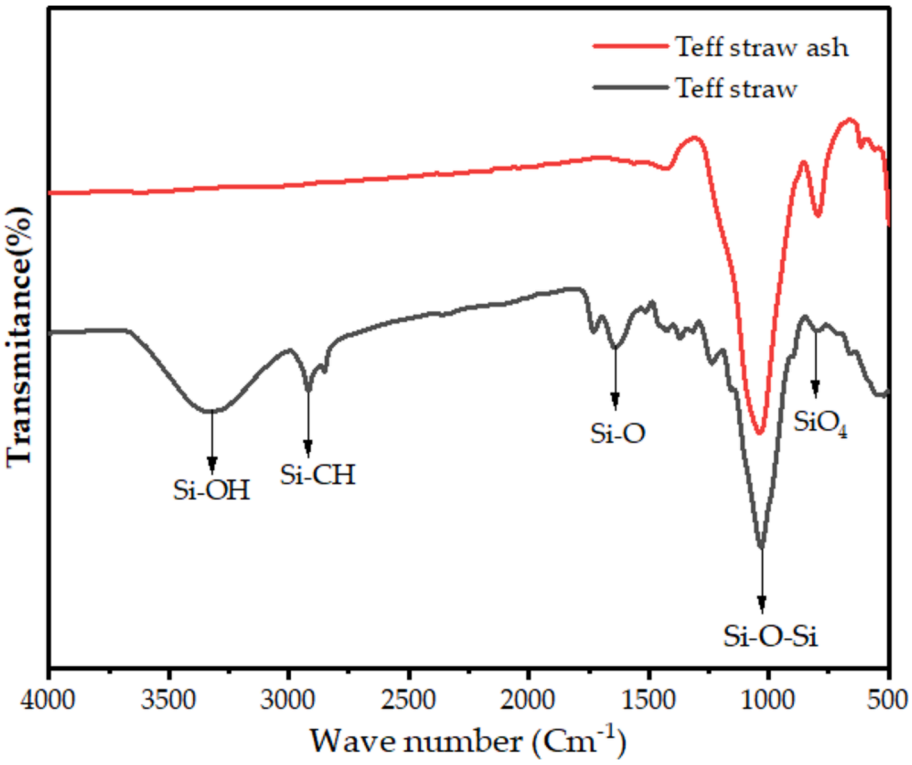

Fig. 2. FTIR spectra of teff straw of Flagot variety.

3.5. Yield of silica gel

This process is aimed at removing various impurities, including alkali, alkaline earth, and transition metals such as potassium (K), sodium (Na), calcium (Ca), magnesium, aluminum (Al), iron (Fe), and others. These impurities are typically present in the form of salts within the cellular structure or ionically bonded to the lignin or hemicellulose components of the straw (Tessema et al., 2023).

According to Bageru and Srivastava (Bageru and Srivastava, 2018), during the removal of metal contents, there is an increase in the size of the pores, which consequently enhances the pore surface area of the straw. This process is also accompanied by the chemical activation of carbonaceous content. It is used for the removal of ionically bound metals from lignin or hemicellulose. Such activation is beneficial for the removal of both organic and carbonaceous matter during the high-temperature ashing process. It is crucial to address these impurities early on as they can adversely impact the final product's (biosilica gel) critical properties, including porosity, color, specific surface area, morphology, and other fundamental characteristics (Bageru and Srivastava, 2018; Irfan et al., 2022). After the temperature of the mixture was allowed to stabilize at room temperature, Whatman No. 41 ash-less filter paper was employed to facilitate the separation of the acid-treated TS from the residual wastewater. The resultant solid was subjected to repeated rinsing using distilled water until it reached a pH that is considered neutral. Subsequent to the washing procedure, the sample was subjected to desiccation utilizing a hot air oven, followed by preservation in a polyethylene container, earmarked for subsequent ashing procedures.

To assess the influence of thermal conditions and duration of calcination on the efficiency of silica gel production, Eq. (3) was employed. The quantification of silica gel was performed using a starting quantity of 10 g of TSA. Eq. (3) facilitated the evaluation of the amount of silica gel successfully synthesized from TSA (Tessema et al., 2023).

$$\text{Silica gel yield} = \frac{m_{SG}}{m_{TSA}} * 100\% \quad (3)$$

where, m_{SG} is mass of silica gel obtained after extraction and m_{TSA} is the mass of TSA.

The exploration of TSA's potential for silica gel production revealed significant findings. The impact of varying ashing temperatures and calcination durations was meticulously evaluated by measuring the silica gel yield through Eq. (3). An impressive yield of 94.2 % was recorded, indicating a robust production process. Notably, the precursors sourced from Debre Zeit Research Center outperformed those obtained from local farmers, with previous studies showing yields ranging from 49.5-84.5 % (Bageru and Srivastava, 2018) and 59.38–85.85 % (Amibo et al., 2022.). This indicates that the methodologies currently in use at the research facility are remarkably effective in producing silica gel, potentially establishing a new standard for subsequent research.

3.6. Surface area, pore volume and pore size using BET method

Pore size, pore volume, and BET surface area were measured from the ashes of teff straw in order to analyze the MSG. For comparison, the surface area, pore diameter, and pore volume of an additional silica aerogel are also given. With a modifier ratio of TMCS/ethanol/hexane of 15/25/100, 25/25/100, 35/25/100, and 50/25/100, respectively, the surface area of MSG today varies from 393.7, 510.4, 475.9, and 331.1 m^2/g. Reports state that teff straw ash generated MSG at a 25/25/100 modification with a surface area greater than that of other feedstocks. like the husk of rice (280 m^2/g) (Thamilselvi and Radha, 2017; Tessema et al., 2023). This indicates that teff straw ash is one of the possible precursors to the production of MSG.

3.7. Analysis using UV–vis spectroscopy

Both the existence of AgNps and amino groups on the silica surface was confirmed by the absorbance (a.u.) vs absorption peaks at 325 nm for the samples containing 1.5, 3, 6, and 9 mM AgNps presented in Fig. 3. The near UV absorption peak in the 240–400 nm region was likewise

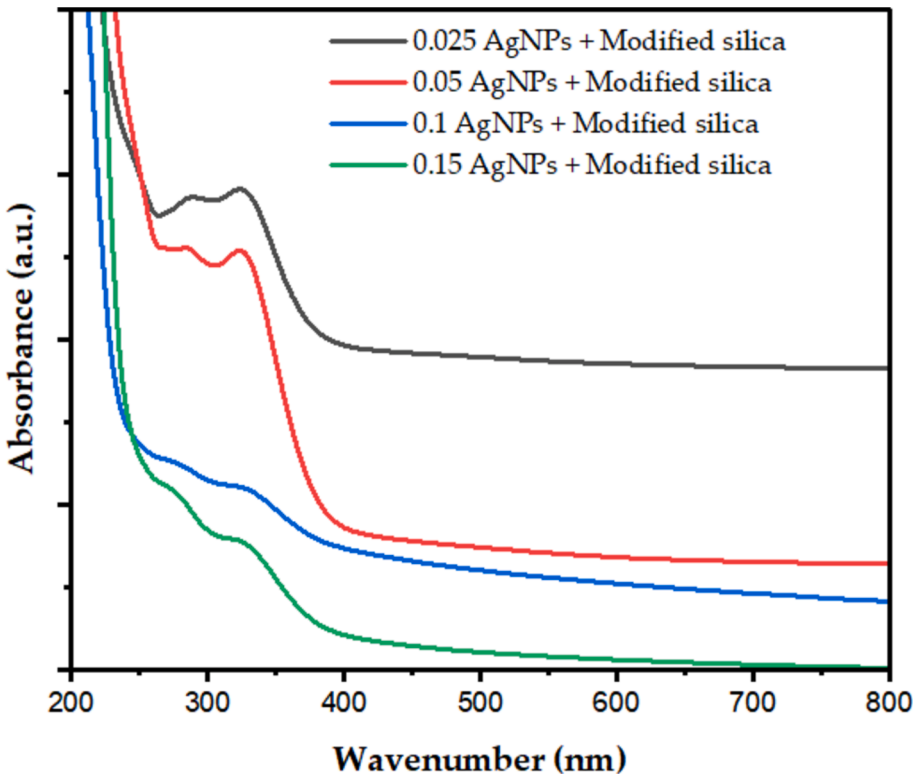

Fig. 3. The UV–vis absorption spectrum of MSG supported AgNPs synthesized using sol–gel method.

influenced by the amino groups (Zhang et al., 2016). Silver nanoparticles' (AgNPs') surface plasmon resonance collective oscillation of the conduction electrons in response to incident light—determines their optical properties. AgNPs can have their size, shape, and surrounding medium changed to adjust their SPR band. According to earlier research, AgNPs display a distinctive surface photoluminescence peak in the visible spectrum, usually ranging from 400 to 530 nm, contingent upon the stabilizing agent and synthesis technique. AgNPs production and

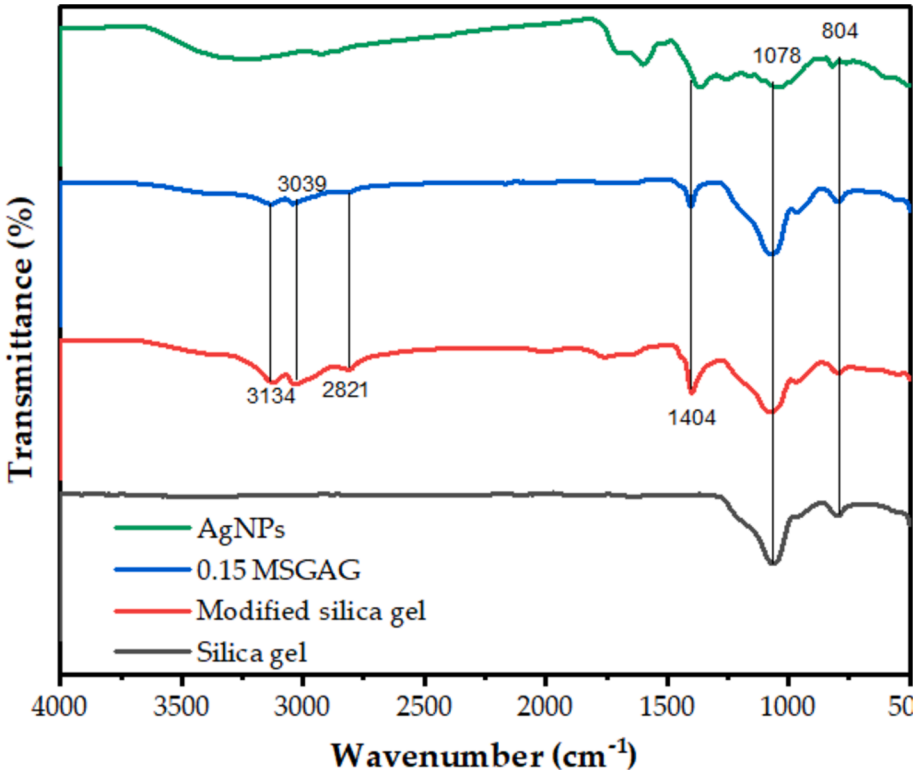

Fig. 4. Results of SG, MSG, and MSG supported at various AgNPs and AgNPs concentrations using FTIR spectra.

presence in a sample can be verified using the SPR peak as a signature. For instance, AgNPs produced with polyvinylpyrrolidone as a capping agent and sodium borohydride as a reducing agent showed an SPR peak at 452 nm in prior research.

3.8. The FT-IR analysis

Fig. 4 displays the FT-IR spectra of the various samples. Two prominent peaks in the silica spectrum can be seen at 1,078 and 804 cm^{-1}, respectively, which represent the symmetric and asymmetric stretching vibrations of Si-O-Si. A new peak at 1,620 cm^{-1} in the MSG spectrum indicates the existence of NH_2 groups on the surface. Because water molecules that have been adsorbed on the nanoparticles exhibit O–H stretching vibrations, a broad band may be seen in the AgNPs spectra at approximately 3,400 cm^{-1}. The features of the MSG and AgNPs spectra are combined in the MSG-supported AgNPs spectrum, indicating that the nanoparticles were successfully immobilized on the silica gel surface (Thamilselvi and Radha, 2017). The strong and weak peaks in the 804–1077 cm^{-1} range identify the Si–O–Si links present in the MSG network. The C–H intensifying peak in the region of 1404 to 3134 cm^{-1} is also caused by the presence of Si-C bonds, which are connected to the TMCS. The absorption band associated with the H-O–H vibrations at around 1770 cm^{-1} indicates the polarity of the MSG (Abdul Halim et al., 2017). The primary bands of the AgNPs absorption spectrum at 3,410 and 1,640 cm^{-1}, respectively, were ascribed to the principal amides and OH stretching vibrations, indicating that phytochemical substances stabilized the silver nanoparticle. The absorption spectrum of AgNPs-loaded silica is shown in Fig. 3, where the C–H peak band is between 1404 and 3134 cm^{-1}. The main amide group, the Si-O-Si stretching vibrations, and the carbonyl group are located at 1,770, 804, and 1650–1850 cm^{-1}, respectively. The band at 900 cm^{-1} was identified as the source of the Si-OH vibration stretching. These absorption peaks demonstrate the AgNPs' electrostatic interaction with the amino group of the functionalized silica gel, functionalizing the amino group and loading AgNPs onto the silica gel's surface. This (Abdul Halim et al., 2016; Thamilselvi and Radha, 2017).

3.9. The XRD analysis

Fig. 5 displays the powder XRD patterns of silica gel, AgNPs, MSG, and MSG-supported AgNPs. The large peak at about 23°, which corresponds to the sample calcined at 700 °C, clearly shows the amorphous character of the silica gel. Sharper peaks in the other samples show the presence of crystalline phases (Chiarakorn et al., 2007). The plant material is the source of the non-crystalline silica gel that is produced by heating teff straw to 700 °C for 2 h. A prominent peak at 2θ of 23° can be seen in the XRD spectra in Fig. 5, suggesting that the silica gel is primarily amorphous in nature (Gu et al., 2015; Khan et al., 2020).

When XRD analysis was performed on the MSG and MSG supported AgNPs samples, all crystalline forms with a prominent peak were found. The framework of the MSG was well-organized. A notable diffraction peak has been seen at 2θ values of 22.96, 27.42, 32.7, 45.32, 46.92, 52.82, 56.72, 58.32, 66.02, and 75.44° in the MSG and MSG-supported AgNPs that were produced using sol–gel. It is possible that the TMCS modifier's partial removal of Si-OH groups during silylation, which enhanced the amount of siloxane connections, led to superior structure development (Thamilselvi and Radha, 2017; Chiarakorn et al., 2007; Bilgic et al., 2022). The peaks on the MSG and MSG supported AgNPs have been found to be caused by the Cl- from TMCS injected during the surface modification procedure and the Na + from sodium hydroxide solution (Wu et al., 2018; Khan et al., 2020). The Scherrer Eq. (4) was employed to compute the crystalline size of AgNPs by an equation. The computed AgNPs had an average crystallographic size of 29.18 nm (Tessema et al., 2023). These results validated the application of AgNPs on silica gel.

$$D(nm) = \frac{(k)*(\lambda)}{(\beta)*(\cos\theta)} \quad (4)$$

where, k = 0.90, is 0.154 nm, and angle are the values for FWHM (Full width at half-maximum).

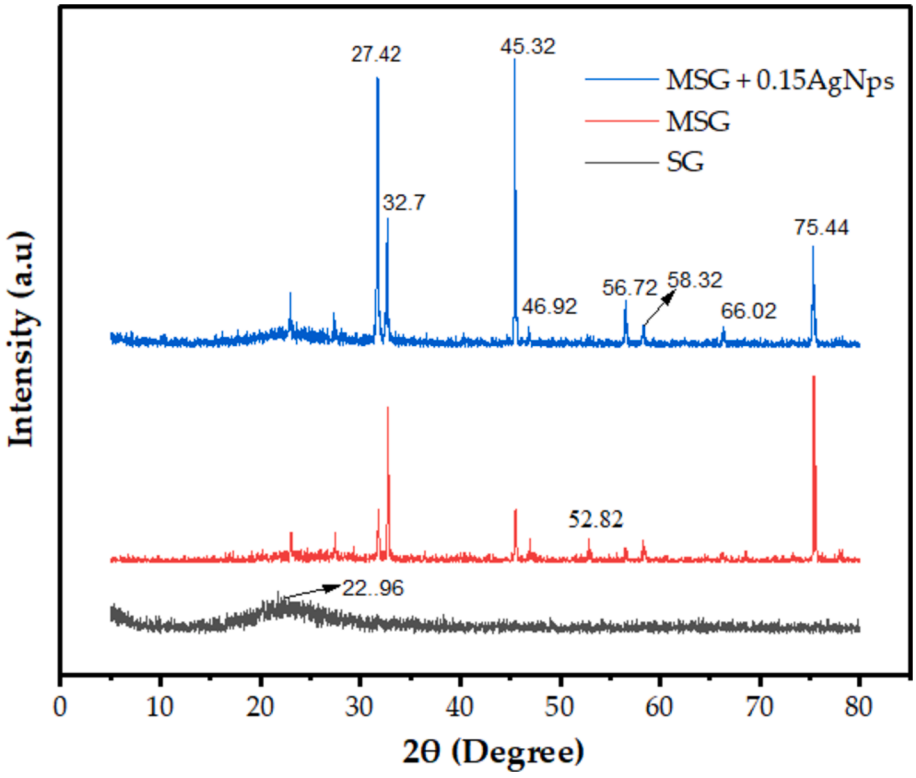

Fig. 5. Results of XRD of SG, MSG and MSG supported at different concentration of AgNPs.

3.10. SEM/EDX analysis

The observations described suggest a complex interaction of materials and conditions. The larger dimensions and glossy surfaces with dark hues indicate a certain level of absorption and reflection of light, which could be intrinsic to the material's composition or a result of specific treatments applied. Alkaline-treated silica gel tends to cluster due to the presence of sodium silicate. It can lead to gelation and the formation of a solid structure with varying degrees of porosity. This clustering is contrasted by the uneven distribution of particles in the presence of a hazardous agent, possibly due to the irregular breakdown of the material's structure. Incomplete combustion is evidenced by carbon impurities, the presence of holes, and hollow structures. Therefore, in Fig. 6 (a), it is typically characterized by this. These findings are critical for understanding the chemical and physical behaviors of materials under different conditions and can have implications for their applications in various fields, including material science and environmental studies. Understanding these interactions is essential for optimizing processes such as the synthesis of silica gels and assessing the environmental impact of combustion-related activities.

The SEM images in Fig. 6(b and c) provide a detailed view of the MSG surface, which has been further enhanced with AgNPs. A honeycomb-like structure with varying pore sizes was observed on the surface. It is a common characteristic that has been found in similar studies. Therefore, this indicates a successful modification process. This modification was also confirmed using SEM images. Additionally, the SEM instrument's capability for energy-dispersive X-ray (EDX) analysis complements the morphological study by allowing for the elemental composition analysis of the silica gel, MSG, and MSG-supported 9 mM AgNPs sample, thereby providing a comprehensive understanding of the three structural and compositional aspects of the material. The incorporation of AgNPs into MSG is a notable advancement in the field of materials science, particularly for applications requiring antibacterial properties. The minor peak of Ag was observed in Fig. 6(c), which confirms the successful modification of the silica gel with silver nanoparticles. This modification has been further corroborated by the EDS analysis of the SEM spectrum. which shows a significant presence of silicon and oxygen, the primary constituents of silica. The presence of silver nanoparticles on the surface of the silica gel could potentially enhance its functionality, opening up new possibilities for its use in various industrial and medical applications (Utama et al., 2019; Abdullah et al., 2023; Khan et al., 2020).

The SEM-EDS spectrum analysis is a crucial step in understanding the composition of precipitated silica gel. It reveals that impurities such as

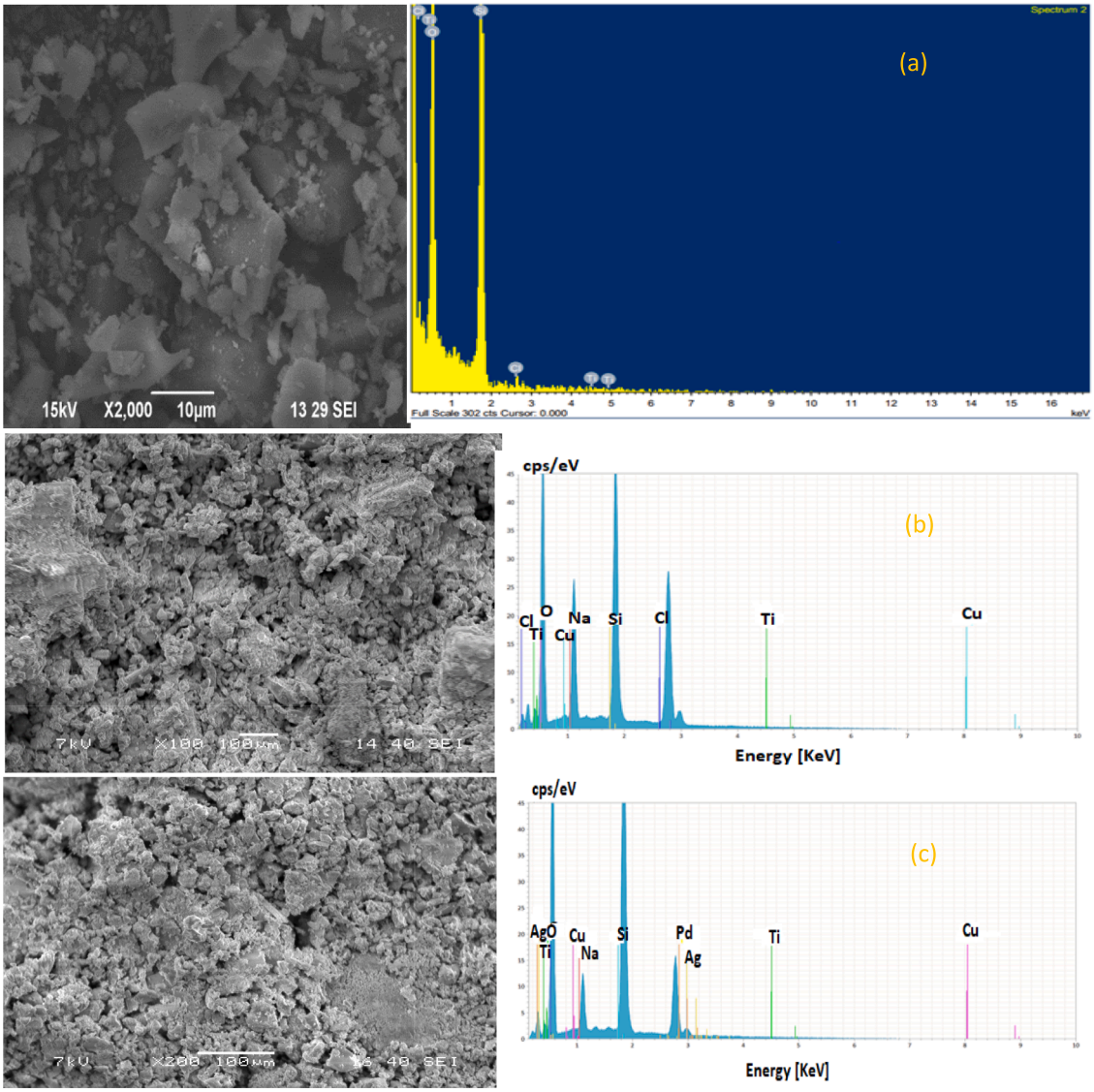

Fig. 6. SEM/EDX image. (a) silica gel (b) TMCS MSG with APD (c) MSG supported AgNPs.

chlorine, titanium, copper, and sodium are present, which can originate from various sources during the manufacturing process. Elements of potassium and aluminum are derived from teff straw. The presence of these elements can significantly influence the physical and chemical properties of the final silica gel product (Utama et al., 2019).

3.11. Technique of the inhibition zone on cell attachment and death

The synthesis of silver nanoparticles (AgNPs) supported by MSG represents a significant advancement in the field of antibacterial agents. By testing these AgNPs against *E. coli* and *S. aureus* at varying concentrations, we can determine the halts of bacterial growth. The zone of inhibition method is a classic microbiological technique that visually demonstrates the antibacterial activity of the AgNPs. It involves measuring the clear area, devoid of bacterial growth, surrounding the AgNPs on a culture plate. This area indicates the effectiveness of the nanoparticles in preventing bacterial proliferation. The results from such experiments are crucial for developing new antibacterial compounds and can lead to breakthroughs in combating bacterial infections. With antibiotic resistance on the rise, the need for novel and effective antibacterial agents is more pressing than ever, making this research both timely and essential. Therefore, after synthesizing AgNPs supported with MSG, we tested their antibacterial effects on *E. coli* and *S. aureus* at different concentrations (10, 20, 30, 40, and 50 mg/mL). Then, using the zone of inhibition method, the bactericidal activity was evaluated against bacterial cultures with a density of $1.5*10^8$ CFU/mL. The average inhibitory zone diameter (measured in millimeters) around each bacterial strain's different pellets is displayed in Fig. 7. We found from the experiments that all doses of AgNPs efficiently inhibited *S. aureus* and *E. coli.* In this experiment, sterile distilled water was used as the negative control, while gentamycin was employed as the positive control.

The diameter of the inhibitory zone against *E. coli* and *S. aureus* was used to measure the antibacterial activity of MSG-supported AgNPs. The findings demonstrated that when the concentration of AgNPs and AgNPs supported by MSG grew, so did the inhibitory zone. The highest inhibitory zone diameter for *S. aureus* was 14.30, and the minimum for *E. coli* was 12.80 for the same bacterial concentration. The study's findings demonstrated that the MSG-supported AgNPs were more effective against *S. aureus* than *E. coli* in terms of antibacterial activity. This might be explained by the two bacteria's different cell wall compositions and structures, which have an impact on how susceptible they are to AgNPs. AgNPs can readily pierce the thick peptidoglycan layer of *S. aureus*; however, AgNPs are repelled by the outer membrane of *E. coli.* Additionally, compared to the unmodified AgNPs, the MSG-supported AgNPs had a bigger surface area and a higher silver content, which improved their interaction and contact with the bacterial cells. As a result, the MSG-supported AgNPs may be regarded as a material with promise for use in antibacterial applications against *E. coli* and *S. aureus*. The synthesized AgNPs demonstrated potent antibacterial properties against *E. coli* and *S. aureus*, showcasing their potential for diverse applications in fields like nanomedicine, catalysis, and sensing technologies. Our findings demonstrate that the AgNPs, with an average size of roughly 63.08 nm, are uniformly sized and evenly distributed on the silica surface. Both bacteria's growth is more than 90 % inhibited by the AgNPs, demonstrating their outstanding antibacterial effectiveness. The AgNPs supported by silica have shown greater antibacterial activity against *S. aureus* (13.6 mm) than *E. coli* (11.9 mm), which is consistent with this investigation. Their technique can be used to manufacture AgNPs immobilized on silica for a variety of uses in nanomedicine, catalysis, and sensing. It is easy to use, affordable, and ecologically benign (Dahlous et al., 2019).

According to Table 3 results, silica gel-based composites that have been infused with silver are successful in generating a zone of inhibition that blocks the growth of bacteria. This is a positive result for applications involving bacterial disinfection since it suggests that these composites may be able to successfully stop the growth and spread of bacteria. These kinds of materials might be essential in sterilisation-critical industries, medical settings, and water purification systems. The addition of silver, which has antibacterial qualities, increases the silica gel's effectiveness and makes it a strong option for disinfection.

3.12. Mechanism of AgNPs against pathogenic contaminants

AgNPs have various antibacterial effects, but their exact mechanisms of action are unknown. They release silver ions that can stop bacteria from growing by binding to sulphur containing proteins and amino acids in bacterial cell membranes leads to inactivation of the bacteria on their membranes and walls. Furthermore, the release of silver ions from AgNPs can inhibit enzyme activities by interacting with phosphorus in

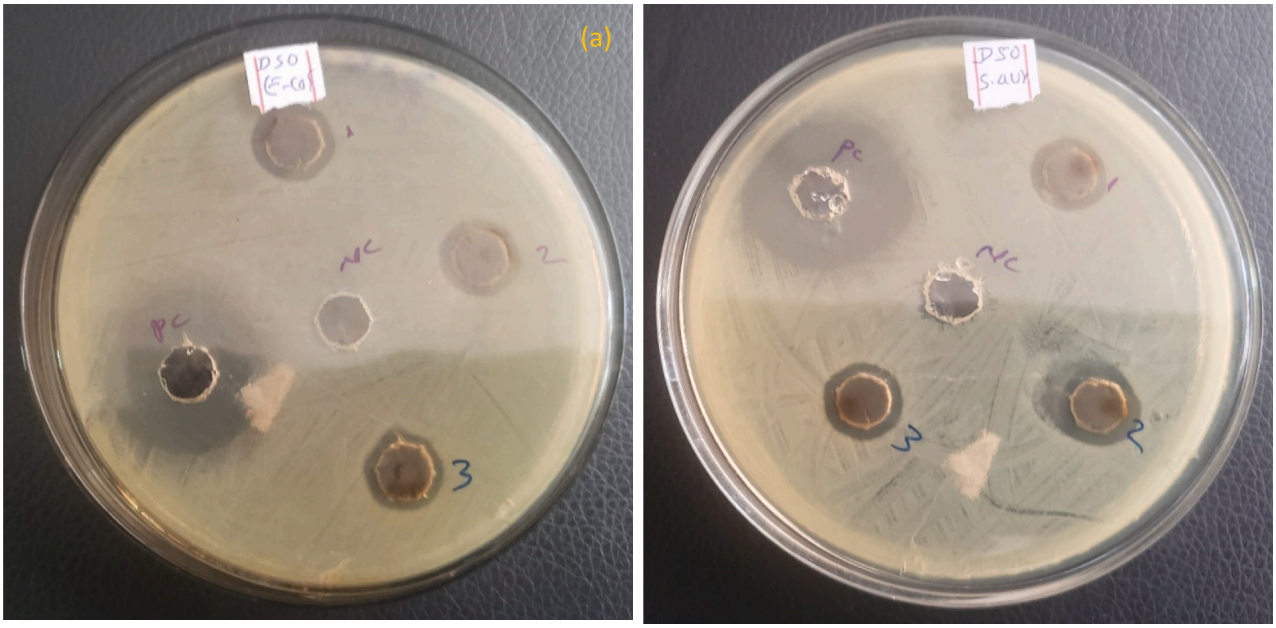

Fig. 7. Zone inhibition of (a and b) *E. coli* and (c and d) *S. aureus* against MSG supported AgNPs.

Table 3
Zone of inhibition tests against bacterial suspension using AgNPs-composite solution as imbibition agent (Tessema et al., 2024).

Bacteria	Material	Inhibition zone diameter (mm)
E. coli	MSG (1.5 gm Ag)	12.80
S. aureus		14.30
E. coli	SG (0.1 gm Ag)	11.9
S. aureus		13.6
E. coli	($AgNO_3$) and SG (1:1, wt/wt)	5.85
S. aureus		6.68
S. aureus		18.2
E. coli	SG-AgNPs	6.3
S. aureus		7.07
E. coli	AgNPs@SG	12
S. aureus		13
C. Albicans		11
E. coli	Ag2@MCM-41	15
S. aureus		13
C. Albicans		12

DNA and sulphur in proteins. As presented in Fig. 8, AgNPs are also indeed known for attributed to their ability to interact with negatively charged biomolecules. When AgNPs come into contact with bacterial cells, they can attach to the cell membrane due to electrostatic attraction, as the cell membrane often carries a negative charge. This interaction can lead to the disruption of the cell membrane's integrity, causing structural changes that can ultimately result in cell death. Additionally, AgNPs can penetrate inside the bacteria, where they may interact with sulfur-containing proteins and phosphorus-containing elements like DNA, leading to further damage. These interactions can inhibit cell replication and lead to the generation of reactive oxygen species, which can also contribute to the bactericidal effect of AgNPs. The precise mechanisms of action are complex and still under investigation, but the ability of AgNPs to induce multiple types of damage to bacterial cells is a key factor in their antimicrobial efficacy (Mukundan et al., 2017; Khan, 2023).

3.13. Future directions of the study

The future directions for the preparation of modified silica gel supported silver nanoparticles for water disinfection are likely to focus on enhancing the efficiency and selectivity of the nanoparticles. Recent studies are exploring the applications of silica-based nanoparticles in various fields, including environmental remediation and wastewater treatment, due to their distinctive physiochemical characteristics. Additionally, there is ongoing research into the broad-spectrum antimicrobial activity of silica gel embedded with silver nanoparticles, which could be crucial for water disinfection applications. The continuous improvement in the synthesis methods and the functionalization of silica nanoparticles will likely lead to more effective solutions for water treatment and other environmental applications. The integration of these nanoparticles into existing water treatment systems and the evaluation of their long-term stability and ecological impact are also critical areas for future research. This will ensure that the nanoparticles are not only effective in disinfecting water but also safe for the

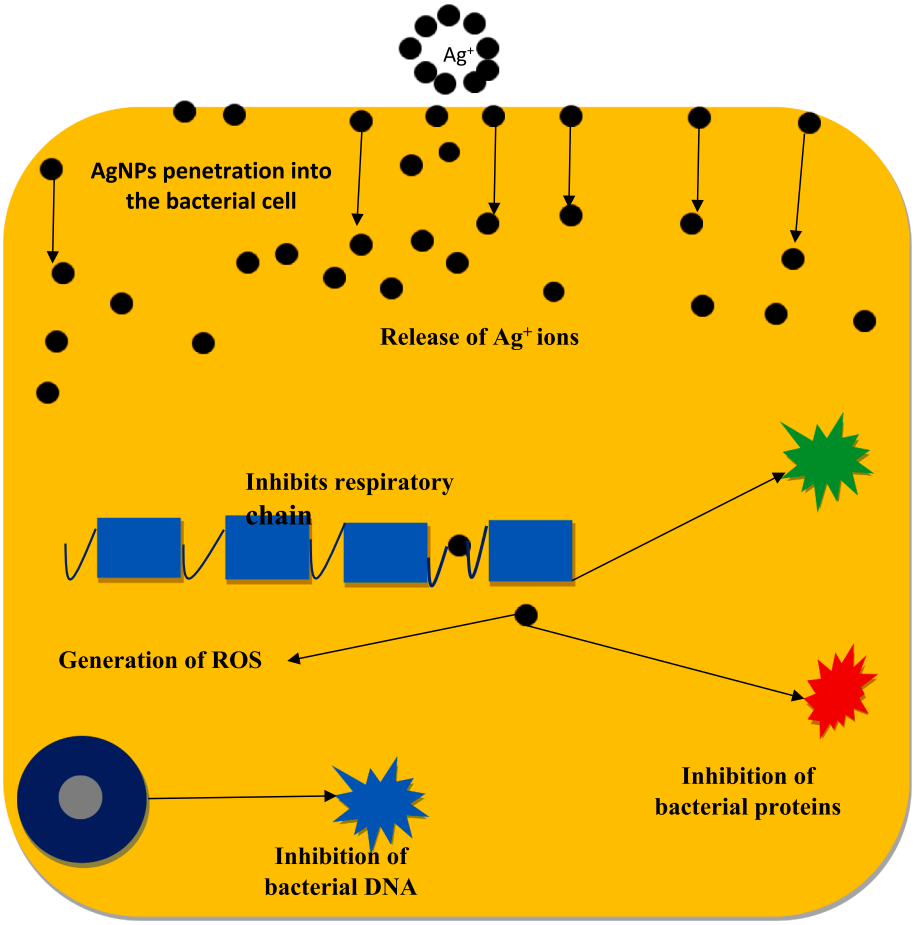

Fig. 8. Proposed mechanism of AgNPs on the surfaces of Gram-positive and Gram-negative bacteria.

environment and public health.

4. Conclusions

In the current study, modified silica gel supported silver nanoparticles (MSG-AgNPs) were synthesized for the treatment of drinking water. AgNPs were synthesized from silver nitrate (AgNO3) solution and Vernonia amygdalina leaf extract for the treatment of drinking water and characterized. AgNPs were synthesized at different concentrations of AgNO3 while keeping the leaf extract solution constant and characterized for their removal efficiency of removing pathogenic microorganisms after being supported by MSG.. Several methods were employed to characterize the characteristics of the MSG-modified AgNPs. BET was used to assess the surface area, whereas UV–Vis spectrophotometry was used to measure size. Crystallinity was evaluated by XRD, and the functional groups were determined by FTIR. Using SEM/EDX, the morphology and elemental content were examined. MSG with a greater specific area can be produced. For synthesized MSG, the ideal volumetric ratio to obtain the maximum practical specific surface area was determined to be 25/25/100. The average pore size was 2.670 nm, the average pore volume was 0.5422 cm3/g, and the specific surface area was 909.250 m2/g. The absorption peaks at 325 nm in the spectra were indicative of the presence of the amino group in the AgNPs-containing silica. The primary chemical groups of the silica gel were Si-O-Si, Si-OH, Si-CH, and Si-O, based on the FT-IR data. AgNPs were linked to amides and OH stretching vibrations, whereas the presence of C–H groups suggested MSG. The results of the XRD research showed that silica was found in all of the AgNPs supported by MSG, silica gel, and MSG. The size of the clear region surrounding the MSG with AgNPs on plates with *E. coli* and *S. aureus* was used to gauge the antibacterial impact of the mixture. The impact of the granules' direct interaction with the bacteria may be measured thanks to this technique. The inhibitory zone expanded as contact duration and AgNPs concentration increased, while *E. coli* and *S. aureus* bacterial counts decreased for all employed bacterial concentrations.

CRediT authorship contribution statement

Belete Tessema: Writing – review & editing, Writing – original draft, Methodology, Investigation, Conceptualization. **Girma Gonfa:** Writing – review & editing, Visualization, Supervision, Methodology, Investigation. **Sintayehu Mekuria Hailegiorgis:** Formal analysis, Investigation, Supervision, Writing – review & editing.

Declaration of Competing Interest

The authors declare that they have no known competing financial interests or personal relationships that could have appeared to influence the work reported in this paper.

Acknowledgement

This work was financially supported by Addis Ababa Science and Technology University, Ethiopia internal research grant (IGP 006/2023).

References

Abdul Halim, Z.A., Mat Yajid, M.A. Hamdan, H., editors. Synthesis and characterization of rice husk ash derived-silica aerogel beads prepared by ambient pressure drying. Key Engineering Materials; 2016: Trans Tech Publ.

Abdul Halim, Z.A., Mat Yajid, M.A., Idris, M.H., Hamdan, H., 2017. Effects of silica aerogel particle sizes on the thermal–mechanical properties of silica aerogel–unsaturated polyester composites. Plast., Rubber Compos. 46 (4), 184–192.

Abdullah, A., Kursunlu, A.N. Guler, E. A high-performance fluorescent hybrid material for fluorometric detection and removal of toxic Pb (ii) ions from aqueous media: performance and challenges.*RSC advances*, 13 (4) (2023) 2683-91.

Alegbeleye, O.O., Sant'Ana, A.S., 2020. Manure-borne pathogens as an important source of water contamination: An update on the dynamics of pathogen survival/transport as well as practical risk mitigation strategies. Int. J. Hyg. Environ. Health 227, 113524.

Amibo, T.A., Beyan, S.M., Damite, T.M., 2022.. Production and optimization of bio-based silica nanoparticle from teff straw (eragrostis tef) using rsm-based modeling, characterization aspects, and adsorption efficacy of methyl orange dye. J. Chem. 2022.

Anjum, N., Khan, W., Hobiny, A., Azam, M., Waqas, M., Irfan, M., 2022. Numerical analysis for thermal performance of modified Eyring Powell nanofluid flow subject to activation energy and bioconvection dynamic.*Case Studies in*. Therm. Eng. 39, 102427.

Asfaw, B.T., Gari, M.T., Jayakumar, M., Baskar, G., 2024. Sustainable Bioethanol Production from the Pretreated Waste Lignocellulosic Feedstocks. Circular Bioeconomy Perspectives in Sustainable Bioenergy Production: Springer 377–394.

ASTM, ASTM D-3174-93-Standard test method for ash in the analysis sample of coal and coke from coal: Annual Book of ASTM Standards; [1988].

Azarang, M., Bakhtiyari, A., Rakhshani, R., Davarpanah, A.M., Aliahmad, M., Jahantigh, M.F., 2021. Green gelatin-assisted: Synthesis of Co3O4NPs@ rGO nanopowder for highly efficient magnetically separable methylene orange dye degradation. Adv. Powder Technol. 32 (2), 504–514.

Bageru, A.B., Srivastava, V., 2017. Preparation and characterisation of biosilica from teff (eragrostis tef) straw by thermal method. Mater. Lett. 206, 13–17.

Bageru, A.B., Srivastava, V.C., 2018. Biosilica preparation from abundantly available African biomass Teff (Eragrostis tef) straw ash by sol-gel method and its characterization. Biomass Convers. Biorefin. 8 (4), 971–978.

Bilgic, A., Cimen, A., Kursunlu, A.N., Karapınar, H.S., Guler, E., 2022. Synthesis, characterization, and application of functionalized pillar [5] arene silica gel (Si-APTMS-pillar [5] arene) adsorbent for selectivity and effective removal of Cu (II) ion. J. Mater. Res. 37 (21), 3587–3598.

Bilgic, A., Cimen, A. Kursunlu, A.N. "Killing two birds with one stone": A fluorescent hybrid nanoparticle modified with BODIPY for efficiently detection and removal of toxic Cu (II) ion from aqueous solutions.*Science of The Total Environment*, 845 (2022) 157170.

Braschi, I., Blasioli, S., Buscaroli, E., Montecchio, D., Martucci, A., 2016. Physicochemical regeneration of high silica zeolite Y used to clean-up water polluted with sulfonamide antibiotics. J. Environ. Sci. 43, 302–312.

Bruna, T., Maldonado-Bravo, F., Jara, P., Caro, N., 2021. Silver nanoparticles and their antibacterial applications. Int. J. Mol. Sci. 22 (13), 7202.

Chiarakorn, S., Areerob, T. Grisdanurak, N. Influence of functional silanes on hydrophobicity of MCM-41 synthesized from rice husk.*Science and Technology of Advanced Materials*, 8 (1-2) (2007) 110.

Dahlous, K.A., Abd-Elkader, O.H., Fouda, M.M., Al Othman, Z., El-Faham, A., 2019. Eco-friendly method for silver nanoparticles immobilized decorated silica: synthesis & characterization and preliminary antibacterial activity. J. Taiwan Inst. Chem. Eng. 95, 324–331.

Designation, A. D 3175 Standard Test Method for Volatile Matter in the Analysis Sample of Coal and Coke.*Annual Book of Standards. PA: ASTM. USA*, (2017).

Ding, Y., Su, D., 2012. Purifying Native in-Situ Mastoid SiO2 from Rice Husk. Energy Procedia 16, 1269–1274.

El-Aassar, A.H., Said, M., Abdel-Gawad, A., Shawky, H., 2013. Using silver nanoparticles coated on activated carbon granules in columns for microbiological pollutants water disinfection in abu rawash area, great cairo egypt. Australian J. Basic and Appl. Sci. 7 (1), 422–432.

Feng, Q., Chen, K., Ma, D., Lin, H., Liu, Z., Qin, S., Luo, Y., 2018. Synthesis of high specific surface area silica aerogel from rice husk ash via ambient pressure drying. Colloids Surf A Physicochem Eng Asp 539, 399–406.

Gari, M.T., Asfaw, B.T., Abo, L.D., Jayakumar, M., Kefalew, G., 2024. Effective Utilization of Agricultural Cereal Grains in Value-Added Products: A Global Perspective. Springer, Value Added Products From Food Waste, pp. 41–58.

González-Castaño, M., De Miguel, J.N., Sinha, F., Wabo, S.G., Klepel, O., Arellano-Garcia, H., 2021. Cu supported Fe-SiO2 nanocomposites for reverse water gas shift reaction. Journal of CO2 Utilization 46, 101493.

Gu, S., Zhou, J., Yu, C., Luo, Z., Wang, Q., Shi, Z., 2015. A novel two-staged thermal synthesis method of generating nanosilica from rice husk via pre-pyrolysis combined with calcination. Ind. Crop. Prod. 65, 1–6.

Gurav, J.L., Rao, A.V., Rao, A.P., Nadargi, D., Bhagat, S., 2009. Physical properties of sodium silicate based silica aerogels prepared by single step sol–gel process dried at ambient pressure. Journal of Alloys and Compounds 476 (1–2), 397–402.

Hussain, Z. Azeem Khan, W. Impact of thermal-solutal stratifications and activation energy aspects on time-dependent polymer nanoliquid.*Waves in random and complex media*, (2022) 1-11.

International, A., 2017. ASTM D3173/D3173M-17a Standard Test Method for Moisture in the Analysis Sample of Coal and Coke: ASTM International West Conshohocken. PA, USA.

Irfan, M., Khan, W., Pasha, A.A., Alam, M.I., Islam, N., Zubair, M., 2022. Significance of non-Fourier heat flux on ferromagnetic powell-eyring fluid subject to cubic autocatalysis kind of chemical reaction. Int. Commun. Heat Mass Transfer 138, 106374.

Khan, W., Ali, M., Irfan, M., Khan, M., Shahzad, M., Sultan, F., 2020. A rheological analysis of nanofluid subjected to melting heat transport characteristics. Appl. Nanosci. 10, 3161–3170.

Khan, W., Ali, M., Shahzad, M., Sultan, F., Irfan, M., Asghar, Z., 2020. A note on activation energy and magnetic dipole aspects for Cross nanofluid subjected to cylindrical surface. Appl. Nanosci. 10, 3235–3244.

Khan, W., Sun, H., Shahzad, M., Ali, M., Sultan, F., Irfan, M., 2021. Importance of heat generation in chemically reactive flow subjected to convectively heated surface. *Indian*. J. Phys. 95, 89–97.
Khan, W., Anjum, N., Waqas, M., Abbas, S., Irfan, M., Muhammad, T., 2021. Impact of stratification phenomena on a nonlinear radiative flow of sutterby nanofluid. J. Mat. Research Techn. 15, 306–314.
Khan, W., Ahmad, A., Anjum, N., Abbas, S., Chammam, W., Riahi, A., Rebei, H., Zaway, M., 2022. Impact of nanoparticles and radiation phenomenon on viscoelastic fluid. Int. J. Mod Phys B 36 (05), 2250049.
Khan, W., Arshad, Z., Hobiny, A., Saleem, S., Al-Zubaidi, A., Irfan, M., 2022. Impact of magnetized radiative flow of sutterby nanofluid subjected to convectively heated wedge. Int. J. Mod Phys B 36 (16), 2250079.
Khan, W.A., Waqas, M., Kadry, S., Asghar, Z., Abbas, S.Z., Irfan, M., 2020. On the evaluation of stratification based entropy optimized hydromagnetic flow featuring dissipation aspect and robin conditions. Comp. Meth. Prog. Biomed. 190, 105347.
Khan, W.A., Waqas, M., Chammam, W., Asghar, Z., Nisar, U.A., Abbas, S.Z., 2020. Evaluating the characteristics of magnetic dipole for shear-thinning Williamson nanofluid with thermal radiation. Comp. Meth. Prog. Biomed. 191, 105396.
Khan, W.A. Significance of magnetized Williamson nanofluid flow for ferromagnetic nanoparticles.*Waves in Random and Complex Media*, (2023) 1-20.
Khan, W.A. Dynamics of gyrotactic microorganisms for modified Eyring Powell nanofluid flow with bioconvection and nonlinear radiation aspects.*Waves in Random and Complex Media*, (2023) 1-11.
Khojasteh-Taheri, R., Ghasemi, A., Meshkat, Z., Sabouri, Z., Mohtashami, M., Darroudi, M., 2023. Green Synthesis of Silver Nanoparticles Using Salvadora persica and Caccinia macranthera Extracts. In: Cytotoxicity Analysis and Antimicrobial Activity against Antibiotic-Resistant Bacteria. Applied Biochemistry and Biotechnology, pp. 1–16.
Mohamad, N.F., Rani, N.H.A., Elham, O.S.J., Muhamad, S.H.A., Muda, S.A., Basear, Y. Faisal, M.K.M., editors. Synthesis and characterization of silica aerogel from rice husk with ambient pressure drying method. Journal of Physics: Conference Series; 2020: IOP Publishing.
Morales-Paredes, C.A., Rodríguez-Linzán, I., Saquete, M.D., Luque, R., Osman, S.M., Boluda-Botella, N., Manuel, R.-D.-J., 2023. Silica-derived materials from agro-industrial waste biomass: Characterization and comparative studies. Environ. Res. 231, 116002.
Mukundan, D., Mohankumar, R., Vasanthakumari, R., 2017. Comparative study of synthesized silver and gold nanoparticles using leaves extract of Bauhinia tomentosa Linn and their anticancer efficacy. Bulletin Mater. Sci. 40, 335–344.
Murugadoss, S., Lison, D., Godderis, L., Van Den Brule, S., Mast, J., Brassinne, F., Sebaihi, N., Hoet, P.H., 2017. Toxicology of silica nanoparticles: an update. Arch. Toxicol. 91 (9), 2967–3010.
Neme, I., Gonfa, G., Masi, C., 2023. Castor seeds hull activated carbon impregnated with silver nanoparticles for removal of Escherichia coli from water. Case Studies in Chemical and Environmental Engineering 7, 100320.
Norsuraya, S., Fazlena, H., Norhasyimi, R., 2016. Sugarcane bagasse as a renewable source of silica to synthesize santa barbara amorphous-15 (SBA-15). Procedia Eng. 148, 839–846.
Ojha, A., 2020. Nanomaterials for removal of waterborne pathogens Opportunities and Challenges. Waterborne Pathogens 385–432.
Parandhaman, T., Das, A., Ramalingam, B., Samanta, D., Sastry, T., Mandal, A.B., Das, S. K., 2015. Antimicrobial behavior of biosynthesized silica–silver nanocomposite for water disinfection: a mechanistic perspective. J. Hazard. Mater. 290, 117–126.
Payami, R., Ghorbanpour, M.P., Jadid, A., 2016. Antibacterial silver-doped bioactive silica gel production using molten salt method. Journal of Nanostructure Chemistry 6 (3), 215–221.
Phong, N.T.P., Thanh, N.V.K. Phuong, P.H., editors. Fabrication of antibacterial water filter by coating silver nanoparticles on flexible polyurethane foams. Journal of Physics: Conference Series; 2009: IOP Publishing.
Quang, D.V., Sarawade, P.B., Hilonga, A., Kim, J.-K., Chai, Y.G., Kim, S.H., Ryu, J.-Y., Kim, H.T., 2011. Preparation of amino functionalized silica micro beads by dry method for supporting silver nanoparticles with antibacterial properties. Colloids Surf A Physicochem Eng Asp 389 (1–3), 118–126.
Quang, D.V., Sarawade, P.B., Jeon, S.J., Kim, S.H., Kim, J.-K., Chai, Y.G., Kim, H.T., 2013. Effective water disinfection using silver nanoparticle containing silica beads. Appl. Surf. Sci. 266, 280–287.
Raanan, R., Zack, O., Ruben, M., Perluk, I., Moshe, S., 2022. Occupational Silica Exposure and Dose-Response for Related Disorders—Silicosis, Pulmonary TB, AIDs and Renal Diseases: Results of a 15-Year Israeli Surveillance. Int. J. Environ. Res. Public Health 19 (22), 15010.
Rahmanifar, E., Azarang, M., Aliahmad, M., 2024. Efficient Photodegradation of Rhodamine B Dye Assisted by Pigskin-Gel via Sustainable Synthesis of Fe2O3@ rGO Nanocrystals with Magnetically Separable Properties. Journal of Sol-Gel Science and Technology 111, 671–688.
Sarker, M.Z., Rahman, M.M., Minami, H., Suzuki, T., Hossain, M.K., Ahmad, H., 2021. Mesoporous amine functionalized SiO2 supported Cu nanocatalyst and a kinetic-mechanistic degradation study of azo dyes. Colloids Surf A Physicochem Eng Asp 617, 126403.
Satlin, M.J., Lewis, J.S., Weinstein, M.P., Patel, J., Humphries, R.M., Kahlmeter, G., Giske, C.G. Turnidge, J. Clinical and Laboratory Standards Institute and European Committee on Antimicrobial Susceptibility Testing position statements on polymyxin B and colistin clinical breakpoints.*Clinical Infectious Diseases*, 71 (9) (2020) e523-e9.
Shayo, G.M., Elimbinzi, E., Shao, G.N., Fabian, C., 2023. Severity of Waterborne Diseases in Developing Countries and the Effectiveness of Ceramic Filters for Improving Water Quality. Bull. Natl. Res. Cent. 47 (1), 113.
Shin, Y.-S., Park, M., Kim, H.-Y., Jin, F.-L., Park, S.-J., 2014. Synthesis of silver-doped silica-complex nanoparticles for antibacterial materials. Bull. Kor. Chem. Soc. 35 (10), 2979–2984.
Tabrez, M. Azeem Khan, W. Exploring physical aspects of viscous dissipation and magnetic dipole for ferromagnetic polymer nanofluid flow.*Waves in random and complex media*, (2022) 1-20.
Tesfaye Gari, M., Tessema Asfaw, B., Arumugasamy, S.K., Deso Abo, L., Jayakumar, M., 2023. Natural resources-based activated carbon synthesis. Encyclopedia of Green Materials: Springer 1–11.
Tessema, B., Gonfa, G., Hailegiorgis, S.M. Prabhu, S.V. Synthesis and characterization of biosilica gel produced from teff (Eragrostis tef) straw using the sol-gel technique. *Bioresource Technology Reports*, (2023) 101497.
Tessema, B., Gonfa, G., Hailegiorgis, S.M., Prabhu, S.V., Manivannan, S., 2023. Synthesis and characterization of silver nanoparticles using reducing agents of bitter leaf (Vernonia amygdalina) extract and tri-sodium citrate. Nano-Struct. Nano-Objects 35, 100983.
Tessema, B., Gonfa, G., Hailegiorgis, S.M., Prabhu, S.V., 2023. Characteristic investigations on bio-silica gel prepared from teff (eragrostis tef) straw: effect of calcination time. Mater. Res. Express 10 (11), 115102.
Tessema, B., Gonfa, G., Hailegiorgis, S.M., Prabhu, S.V., 2023. Synthesis and characterization of biosilica gel produced from teff (Eragrostis tef) straw using the sol-gel technique. Bioresour. Technol. Rep. 22, 101497.
Tessema, B., Gonfa, G., Hailegiorgis, S.M., Sundramurthy, V.P., 2023. Characterization of teff straw from selected teff varieties from Ethiopia. Heliyon 9 (6).
Tessema, B., Gonfa, G., Mekuria Hailegiorgis, S., Venkatesa Prabhu, S., 2023 (2023).. An overview of current and prognostic trends on synthesis, characterization. And Applications of Biobased Silica.*Advances in Materials Science and Engineering*.
Tessema, B., Gonfa, G., Hailegiorgis, S.M., Workneh, G.A., Tadesse, T.G., 2024. Synthesis and evaluation of the anti-bacterial effect of modified silica gel supported silver nanoparticles on E. coli and S. aureus. Results Chemistry 7, 101471.
Tessema, B., Gonfa, G., Hailegiorgis, S.M., Prabhu, S.V., 2024. Synthesis and Characterization of Modified Silica Gel from Teff Straw Ash Using Sol-gel Method. Next Materials 3, 100146.
Tessema, B., Gonfa, G., Hailegiorgis, S.M., 2024. Synthesis of Modified Silica Gel Supported Silver Nanoparticles for the Application of Drinking Water Disinfection: A Review. *Results*. Engineering, 102261.
Thamilselvi, V., Radha, K.V., 2017. Silver nanoparticle loaded silica adsorbent for wastewater treatment. Korean J. Chem. Eng. 34, 1801–1812.
Thamilselvi, V., Radha, K.V., 2017. Silver nanoparticle loaded silica adsorbent for wastewater treatment. Korean J. Chem. Eng. 34 (6), 1801–1812.
Utama, P.S., Yamsaengsung, R., Sangwichien, C., 2019. Production and characterization of precipitated silica from palm oil mill fly ash using CO 2 impregnation and mechanical fragmentation. Braz. J. Chem. Eng. 36, 523–530.
Wang, L., He, H., Zhang, C., Sun, L., Liu, S., Yue, R., 2014. Excellent antimicrobial properties of silver-loaded mesoporous silica SBA-15. J. Appl. Microbiol. 116 (5), 1106–1118.
Waqas, M., Khan, W., Pasha, A.A., Islam, N. Rahman, M.M. Dynamics of bioconvective Casson nanoliquid from a moving surface capturing gyrotactic microorganisms, magnetohydrodynamics and stratifications.*Thermal Science and Engineering Progress*, 36 (2022) 101492.
Wu, X., Fan, M., Mclaughlin, J.F., Shen, X., Tan, G., 2018. A novel low-cost method of silica aerogel fabrication using fly ash and trona ore with ambient pressure drying technique. Powder Technol. 323, 310–322.
Zhang, X.-F., Liu, Z.-G., Shen, W., Gurunathan, S., 2016 1534.. Silver Nanoparticles: Synthesis, Characterization, Properties, Applications, and Therapeutic Approaches. Int. J. Mol. Sci. 17 (9).